



This is a repository copy of *Effects of catalyst agglomerate shape in polymer electrolyte fuel cells investigated by a multi-scale modelling framework*.

White Rose Research Online URL for this paper:  
<http://eprints.whiterose.ac.uk/111443/>

Version: Accepted Version

---

**Article:**

Ismail, M.S., Ingham, D.B., Ma, L. et al. (2 more authors) (2017) Effects of catalyst agglomerate shape in polymer electrolyte fuel cells investigated by a multi-scale modelling framework. *Energy*, 122. pp. 420-430. ISSN 0360-5442

<https://doi.org/10.1016/j.energy.2017.01.092>

---

**Reuse**

This article is distributed under the terms of the Creative Commons Attribution-NonCommercial-NoDerivs (CC BY-NC-ND) licence. This licence only allows you to download this work and share it with others as long as you credit the authors, but you can't change the article in any way or use it commercially. More information and the full terms of the licence here: <https://creativecommons.org/licenses/>

**Takedown**

If you consider content in White Rose Research Online to be in breach of UK law, please notify us by emailing [eprints@whiterose.ac.uk](mailto:eprints@whiterose.ac.uk) including the URL of the record and the reason for the withdrawal request.



[eprints@whiterose.ac.uk](mailto:eprints@whiterose.ac.uk)  
<https://eprints.whiterose.ac.uk/>

## **Title Page**

### **Title**

Effects of catalyst agglomerate shape in polymer electrolyte fuel cells investigated by a multi-scale modelling framework

### **Authors**

M.S. Ismail <sup>\*</sup>, D.B. Ingham, L. Ma, K.J. Hughes, and M. Pourkashanian

Energy 2050, Department of Mechanical Engineering, University of Sheffield, Sheffield S3 7RD, UK.

<sup>\*</sup> Corresponding author: Tel: +44 114 21 57242

Email address: m.s.ismail@sheffield.ac.uk (M.S. Ismail)

## **Abstract**

A multi-scale modelling framework is developed for the PEFC cathode electrode. Unlike the conventional agglomerate model, the effects of the microstructure of the agglomerate are numerically coupled to the fuel cell-scale model in this framework. This is performed through solving the agglomerate-scale model first and subsequently extracting and using the data required to generate the performance curves in the fuel cell-scale model. This enables one to freely investigate the structure of the agglomerate without being limited to the only three agglomerate shapes that can be investigated using the conventional agglomerate model: spheres, long cylinders with sealed ends and long slabs with sealed ends. The numerical studies conducted in this work using the developed framework have revealed that the performance of the cathode electrode is highly sensitive to the specific surface area of the agglomerate if the size of the latter is relatively large, i.e. of the order of 1000 nm. Namely, the maximum reported current density has increased by about 60% when changing from the ‘large’ spherical agglomerate to the ‘large’ cylindrical agglomerate. Also, it has been shown that a slight change in the structure of the agglomerate may significantly improve the fuel cell performance.

**Keywords:** PEFCs; Agglomerate model; Multi-scale model; Numerical coupling

## 1. Introduction

The cathode electrode is responsible for the major performance loss in polymer electrolyte fuel cells (PEFCs) and this is primarily due to the sluggish kinetics of the oxygen reduction reaction and the poor utilisation of the conventionally-used platinum-based catalysts [1-3]. In such catalysts, the platinum nanoparticles are supported on carbon black particles which coalesce to form agglomerates [4]. Based on the relevant micrographs, the shape of the above agglomerates normally tend to be semi-spherical [5].

Evidently, the increase in the specific surface area of the catalyst support, which is the ratio between its surface area and volume, leads to an increase in the dispersion and the utilisation of the platinum nanoparticles and the ionomer particles. Equally, it has been demonstrated that the structure of the catalyst support can be controlled using various nano-fabrication techniques [6, 7]. To this end, the structure of the catalyst support can be optimised to maximise the specific surface area of the catalyst support and consequently enhance the dispersion and the utilisation of the catalyst and the ionomer particles. This is expected to improve the performance of the fuel cell and lower the loading of the precious platinum catalysts.

The determination of the optimum structure of the catalyst is often performed through costly and time-consuming experiments [8]. Computational modelling, on the other hand, provides a cost-effective and efficient alternative approach to address the optimisation of the catalyst structure and remarkably reduce the amount of trial-and-error associated with the experimentation [9-11].

The computational PEFC models existing in the literature vary on how the electrodes are treated. The electrodes in some models are treated as interfaces at which the generation and consumption of the species take place, see for example [12-16]. In the other models, the

electrodes are treated as volumes in which the various transport phenomena take place. Under this approach, the models are normally classified as to what are known as homogenous and agglomerate models. The homogenous models assume that the catalyst layer is a porous layer that consists of a uniform mixture of the ionomer, platinum and carbon; see for example [17-27]. On the hand, the agglomerate models assume that the catalyst layer is made up of uniformly distributed isolated agglomerates which consist of a uniform mixture of the ionomer, carbon and platinum; see for example [8, 28-49]. Typically, these agglomerates are assumed to be spherical and covered by a thin ionomer film [28]. The agglomerate models are more realistic than the homogenous models as they (i) account for the dissolution of oxygen into the ionomer phase, and (ii) capture, to a certain extent, the effects of the microstructure of the catalyst agglomerates. However, the incorporation of these effects into the cell-scale numerical models is normally performed analytically through assuming that the shape of the agglomerate is spherical and that the reaction order is one. If the effects of the agglomerate shape are of interest, then one can only investigate three ‘ideal’ shapes using the above classical analytical treatment, namely spheres, long (normally termed as semi-infinite) slabs with sealed ends and long (normally termed as semi-infinite) cylinders with sealed ends [9, 50].

Using the above-mentioned classical agglomerate model, there have been few modelling studies in the literature that have investigated the effects of the shape of the catalyst agglomerate. Jain et al. [35] investigated the effects of the shape of the agglomerate on the performance of a two-dimensional PEFC cathode model. The shapes investigated were the above-mentioned shapes with the same characteristic length, i.e. the spheres, long slabs with sealed ends and long cylinders with sealed ends. All the investigated shapes had the same characteristics length. The characteristic length is the dimension that fixes the size of the agglomerate [51] and is typically obtained by dividing the volume of the agglomerate by its

surface area [50]. Jain et al. [35] found that the best performance was obtained when using the spherical agglomerates. On the other hand, Marthosa [52] developed a one-dimensional numerical model for a PEFC cathode electrode and found that, maintaining the characteristic length constant, the sensitivity of the modelled cathode electrode to the shape of the agglomerate is almost negligible. The discrepancy in the findings of Jain et al. [35] and findings of Marthosa [52] appears to be associated with the specific surface areas used for the agglomerates; Marthosa used the same specific surface area for all the investigated agglomerates whereas the agglomerates in [35] appear to have different specific surface areas. Ismail et al. [9] investigated the effects of the shape of the agglomerate on the performance of a one-dimensional agglomerate. They found that, for a given diffusion path, the slab-like agglomerate outperforms the spherical and cylindrical agglomerate in the low current density region whereas in the high current density region the situation is reversed.

To unlock the limitations associated with the classical agglomerate model, a multi-scale modelling framework is needed. This modelling framework consists of two models: an agglomerate-scale model and a fuel cell-scale model. The agglomerate-scale model is solved using appropriate governing equations and boundary conditions. The outputs from the solved agglomerate-scale model are subsequently numerically linked to the fuel cell-scale model to predict the performance of the latter. Few multi-scale modelling frameworks have been reported in the literature [8, 53]. Kamarajugadda and Mazumder [8] built a three-dimensional agglomerate-scale model and an along-the-channel two-dimensional PEFC model. They generated a look-up table for the current density, changing with overpotential and oxygen concentrations, from the agglomerate-scale model. Subsequently, they computed the current density for the cell-scale model using the look-up table. With this approach, they investigated how the overlapping of the agglomerates affects the performance of the fuel cell. They found that, given that the agglomerates are relatively large, better performance is obtained with the

overlapping two agglomerates than with a single agglomerate of the same volume. Moore et al. [53] developed a one-dimensional model for a spherical agglomerate and a two-dimensional across-the-channel PEFC model. With this multi-scale modelling framework, they investigated the sensitivity of the modelled PEFC to: the order of the oxygen reduction reaction (ORR), agglomerate protonic conductivity and non-equilibrium oxygen dissolution boundary condition.

The conventionally-used carbon black catalyst supports mainly consist of sub- 2 nm pores [6] which are difficult to access by the platinum nanoparticles (~ 2-5 nm) and ionomer polymer matrix (~ 15 nm) [54]; this significantly lowers the utilisation of the catalyst. In an attempt to improve catalyst utilisation, non-conventional carbon and non-carbonaceous catalyst supports have been recently developed, e.g. ordered mesoporous carbons [55], carbon nanotubes [56], graphene and graphene oxides [57] and conducting polymers [58]. Notably, ordered mesoporous carbons feature highly controllable structure, size and pore size and some of the recent relevant experimental studies have shown promising results [59, 60]. However, as mentioned earlier, the experimental nature of these investigations requires a good deal of trial-and-error which render them costly and time-consuming. Given that the appropriate equations and boundary conditions are assigned, multi-scale modelling frameworks can significantly reduce the amount of the trial-and-error through shortlisting the catalyst structures which have the potential to improve the performance of the fuel cell. To this end, the objective of this work is to demonstrate how one can freely investigate the structure of the agglomerate without being limited to the only three shapes dictated by the use of the conventional agglomerate model. Such a flexibility substantially makes the synthesis process of the catalyst more modelling-led and, therefore, significantly saves cost and time.

To meet the above objective, a multi-scale modelling framework has been developed in this paper. In this framework, the current density of the agglomerate-scale model is numerically coupled to the fuel cell-scale model as will be described in the next section. A case study, through which the flexibility of the developed modelling framework is manifested, is presented.

## **2. Methodology**

Two models have been developed to investigate the effects of the structure of the agglomerate on the performance of the fuel cell. The first model represents the catalyst agglomerate and the second model represents the PEFC cathode that is desired to see the effects of the shape of the agglomerate on its performance. The following sections provide details of each model and show how they are linked.

### **Agglomerate-scale Model**

For the purpose of demonstration, three agglomerates with different shapes have been three-dimensionally modelled, namely a sphere, a cube and a long cylinder. Table 1 shows the dimensions of the investigated agglomerates. Note that, to investigate the effect of the agglomerate shape, the dimensions of the cubic and the cylindrical agglomerates were selected to give the same volume as the spherical agglomerate. Each agglomerate was assumed to consist of an active region, where the reaction takes place, and an ionomer film that covers this active region. The active region was assumed to consist of a uniform mixture of the ionomer, carbon and platinum which provides pathways for the protons, dissolved oxygen and electrons to meet and react. The thickness of the ionomer film was set to be 10% of the characteristic length of the agglomerate. For example, the thickness of the ionomer film of the spherical agglomerate was set to be 10 nm (i.e.  $0.1 \times 100$  nm). Some simulations were performed to investigate the effects of slight variation in the thickness of the ionomer

film and such effects were found to be negligible and not affecting the overall findings. Note that small-size agglomerates were initially selected in order for them to be in accordance with the SEM images of the PEFC catalyst layers which show that the size of the semi-spherical catalyst agglomerates is between 100 and 200 nm [5].

**[Insert Table 1]**

It should be noted that the size of carbon black is of the order of 30 nm [6] and therefore assuming a uniform mixture of the ionomer, carbon and platinum when solving the modelled agglomerates (which are of the order of 100-200 nm) may be questionable. However, it was shown that a uniform mixture can be engineered through making use of the advances in the nano-fabrication techniques [59] and therefore assuming continuum when solving the modelled agglomerates is not unrealistic.

The modelled agglomerates were assumed to be isothermal and electrically iso-potential and this is due to the relatively small conduction paths and high electrical and thermal conductivities of the agglomerate materials. Also, using realistic values for the ionic conductivity of the ionomer phase, the agglomerate was shown to be ionically iso-potential [44]. Further, the fuel cell was assumed to operate under low-humidity conditions in order to isolate the effects of saturation. To this end, the only equation solved in the modelled agglomerate is the mass conservation of oxygen:

$$\nabla D_e^{\text{eff}} \nabla C_{\text{O}_2} - R_{\text{rxn}, \text{O}_2} = 0 \quad (1)$$

where  $C_{\text{O}_2}$  is the molar concentration of the dissolved oxygen and  $D_e^{\text{eff}}$  is the effective diffusivity of the dissolved oxygen in the ionomer phase which is given as follows [40]:

$$D_e^{\text{eff}} = \begin{cases} D_e & \text{in the ionomer film} \\ \varepsilon_e^{1.5} D_e & \text{in the active region} \end{cases} \quad (2)$$

where  $D_e$  is the diffusivity of the dissolved oxygen in the pure ionomer and  $\varepsilon_e$  is the volume fraction of the ionomer phase in the active region.  $R_{\text{rxn},\text{O}_2}$  is the oxygen molar consumption rate and is obtained as follows [44]:

$$R_{\text{rxn},\text{O}_2} = \begin{cases} 0 & \text{in the ionomer film} \\ kC_{\text{O}_2} & \text{in the active region} \end{cases} \quad (3)$$

$$k = \frac{i_0 a}{4FC_{\text{O}_2}^{\text{ref}}} \exp\left(\frac{-\alpha F}{RT} \eta\right) \quad (4)$$

where  $k$  is the reaction rate constant,  $i_0$  is the exchange current density,  $F$  is the Faraday's constant,  $C_{\text{O}_2}^{\text{ref}}$  is the reference concentration of the dissolved oxygen,  $\alpha$  is the charge transfer coefficient,  $T$  is the temperature,  $R$  is the universal gas constant and  $\eta$  is the activation over-potential which is the input variable of the model.  $a$  is the specific surface area of the platinum catalyst, i.e. the ratio between the surface area of the platinum particle and its volume and is given by [44]:

$$a = \frac{I_{\text{pt}} A_{\text{pt}}}{L_{\text{cl}}} \quad (5)$$

where  $I_{pt}$  is the platinum loading,  $A_{pt}$  is the electrochemical surface area of the platinum catalyst and  $L_{cl}$  is the thickness of the catalyst layer. The averaged current density of the agglomerate  $\overline{I_{agg}}$  is calculated using Faraday's law:

$$\overline{I_{agg}} = 4Fk\overline{C_{O_2}} \quad (6)$$

where  $\overline{C_{O_2}}$  is the averaged concentration of the consumed dissolved oxygen in the active region of the agglomerate. The boundary conditions used for the model are a specified concentration at the surface of the ionomer film ( $C_{O_2,o}$ ) and symmetry at the centre of the agglomerate. Since a single computational domain is used, the continuity in the flux of the dissolved oxygen at the interface between the ionomer film and the active region is ensured. Fig. 1 shows the implemented boundary conditions on, for example, a cut through the modelled spherical agglomerate.

**[Insert Fig. 1]**

Equation (1) was solved using a finite element software, COMSOL Multiphysics<sup>®</sup> 5.1. The solver used was an iterative linear system solver: GMRES (Generalised Minimum RESidual). The computational domain was discretised and refined, especially near to the interface between the ionomer film and the active region, until a mesh-independent solution is obtained. Specifically, the maximum element size near the above interface was selected to be 0.001  $\mu\text{m}$  with a maximum element growth rate of 1.3. Selection of a smaller maximum element size was found to result in no further improvement. Namely, the maximum current density of the agglomerate was found to reduce by less than 1% when the maximum element

size was reduced from 0.001 to 0.0005  $\mu\text{m}$ ; the corresponding effect on the polarisation curve of the modelled PEFC cathode was found to be negligible. The number of elements used for each computational domain with a mesh-independent solution is about 800K, 780K and 350K for the spherical, cubic and cylindrical agglomerates, respectively. Fig. 2 shows the meshed computational domains for the investigated agglomerates. Note that, due to symmetry, only one eighth of each agglomerate has been modelled.

[Insert Fig. 2]

### PEFC Cathode Model

To isolate the dimensional, thermal and saturation effects, the model was made one-dimensional and the modelled fuel cell was assumed to be isothermal and operating under low humidity conditions. Also, for simplicity, the modelled components were only the GDL and the catalyst layer in the cathode compartment. Fig. 3 shows a schematic diagram of the computational domain. Based on the assumptions given above, only the transport of the chemical species (i.e. oxygen, water vapour and nitrogen) and charge (i.e. electrons and protons) is considered. The transport of the chemical species is described by the following set of equations:

$$\nabla \cdot N_j = S_j \quad (7)$$

where  $N_j$  and  $S_j$  are the mass flux and source term of the species  $j$  (i.e.  $\text{O}_2$ ,  $\text{H}_2\text{O}$  or  $\text{N}_2$ ).

$N_j$  is obtained using the Maxwell-Stefan equation [40]:

$$N_j = -\rho w_j \sum D_{jk}^{\text{eff}} \frac{M}{M_k} \left( \nabla w_k + w_k \frac{\nabla M}{M} \right) \quad (8)$$

$$M = \sum x_j M_j \quad (9)$$

$$\rho = \frac{pM}{RT} \quad (10)$$

where  $\rho$  is the gas mixture density,  $w_j$  and  $w_k$  are the mass fractions of the species  $j$  and  $k$ ,  $x_j$  is the mole fraction of the species  $j$ ,  $M$  is the molecular weight of the gas mixture,  $T$  is the temperature,  $p$  is the pressure and  $D_{jk}^{\text{eff}}$  is the effective diffusivity of the species  $j$  into species  $k$  in the porous media. The Bruggeman approximation was found to significantly over-predict diffusion in the GDL [28]. Therefore, an alternative formula, which reasonably fits the relevant experimental data reported in the literature, was used to calculate the effective diffusivity of the GDL [28]:

$$D_{jk}^{\text{eff}} = 0.008e^{4.81\varepsilon} D_{jk} \quad (11)$$

However, the Bruggeman approximation was still used to calculate the effective diffusivity of the catalyst layer:

$$D_{jk}^{\text{eff}} = \varepsilon_{\text{cl}}^{1.5} D_{jk} \quad (12)$$

For an average pore size of 147 nm [1], Knudsen diffusion in the catalyst layer was found to have negligible effects on the performance of the modelled cathode (not shown) and therefore it was not considered in the simulations. The source term of oxygen in the cathode catalyst layer is equal to the reaction rate of the oxygen consumption  $R_{\text{rxn},\text{O}_2}$  which is, in the cathode electrode, given as follows:

$$R_{\text{rxn},\text{O}_2} = \frac{I}{4F} \quad (13)$$

where  $I$  is the local volumetric local current density and is computed using the solution obtained from the agglomerate-scale as will be described in the next section. The source term of water vapour is given as follows [28]:

$$S_{\text{H}_2\text{O}} = 2R_{\text{rxn},\text{O}_2} + nd\nabla \cdot \mathbf{i} / F \quad (14)$$

where  $nd$  is the net drag coefficient. The activation overpotential was assumed to be constant in the agglomerate-scale model. However, due to the significantly larger length scales, this is not the case in the cathode electrode. To this end, the local activation overpotential  $\eta_{\text{local}}$  is defined as the difference between the solid phase potential  $\phi_s$  and the membrane phase potential  $\phi_m$ :

$$\eta_{\text{local}} = \phi_s - \phi_m \quad (15)$$

The distributions of  $\phi_s$  and  $\phi_m$  within the computational domain are obtained by solving the following conservation of charge equations:

$$\nabla(-\sigma_s^{\text{eff}} \nabla \phi_s) = \nabla \cdot \mathbf{i} \quad \text{in the GDL and CL} \quad (16)$$

$$\nabla(-\sigma_m^{\text{eff}} \nabla \phi_m) = -\nabla \cdot \mathbf{i} \quad \text{in the CL} \quad (17)$$

where  $\sigma_s^{\text{eff}}$  is the effective electrical conductivity of the solid phase (i.e. the GDL and the solid phase in the catalyst layer) and  $\sigma_m^{\text{eff}}$  is the effective membrane conductivity of the

membrane (or ionomer) phase in the catalyst layer. The cell potential  $E_{\text{cell}}$ , which is required for the generation of the polarisation curve, is given as follows:

$$E_{\text{cell}} = E_{\text{th}} - \eta \quad (18)$$

where  $\eta$  is the nominal cathode overpotential which is the difference between the boundary values of the membrane-phase and solid-phase potentials [40] and  $E_{\text{th}}$  is the theoretical cell potential which was calculated using the Nernst equation to be 1.221 V.

Fig. 3 shows the boundary conditions used to solve the model. The concentration boundary conditions were specified at the left side of the domain and zero-flux boundary conditions were specified at the right side of the domain. The boundary conditions of the solid-phase potential were prescribed in a similar manner: a zero solid potential at the left side of the domain and zero-flux boundary condition at the right side of the domain. The conservation of protonic charge equation is only applied to the catalyst layer. To this end, the boundary conditions for the membrane phase potential were as follows: a zero-flux boundary condition at the interface between the GDL and the catalyst layer and a prescribed membrane phase potential at the right side of the domain. It should be noted that, since a single computational domain is used, the continuity boundary conditions at the interface between the GDL and the catalyst layer are ensured for the chemical species and the solid-phase potential. The governing equations of the model, i.e. Equations (7), (16) and (17), were solved using COMSOL Multiphysics<sup>®</sup> 5.1. The solver used was a linear system solver: MUMPS (multifrontal massively parallel sparse direct solver). The domain was discretised and refined especially near the interface between the GDL and the catalyst layer until a mesh-independent solution is obtained. Namely, the maximum element size near the above

interface was selected to be 0.01  $\mu\text{m}$  with a maximum element growth rate of 1.3. Selection of a larger maximum element size, e.g. 0.1  $\mu\text{m}$ , was found to result in an erratic trend at the high current density region of the polarisation curve. On the other hand, selection of a smaller maximum element size, e.g. 0.001  $\mu\text{m}$ , was found to result in negligible change in the values of the current density. The number of the elements used was about 100.

**[Insert Fig. 3]**

### **Coupling**

The  $\overline{I_{\text{agg}}}$  is computed from the agglomerate-scale model and subsequently used to compute the local volumetric current density in the electrode of the PEFC cathode model after being corrected for the porosity of the electrode  $\varepsilon_{\text{cl}}$ .

$$I = \overline{I_{\text{agg}}}(1 - \varepsilon_{\text{cl}}) \quad (19)$$

However, the local current density is a function of the concentration of the dissolved oxygen and the activation overpotential and this is evident from the Butler-Volmer (or Tafel) equation. Therefore, using realistic values for the activation overpotential ( $\eta$ ) and oxygen concentration at the surface of the ionomer film ( $C_{\text{O}_2,\text{o}}$ ), the agglomerate-scale model is repeatedly solved, using the Parametric Sweep utility in COMSOL Multiphysics<sup>®</sup>, to obtain realistic spectrum for  $\overline{I_{\text{agg}}}$  values. These values are subsequently used as an interpolation function to compute the local current density in the PEFC cathode model. Fig. 4 shows  $\overline{I_{\text{agg}}}$  of the spherical agglomerate as a function of both the overpotential and the oxygen concentration at the surface of the ionomer film. To obtain a point in the polarisation curve of the modelled PEFC cathode, the local current density is averaged over the length of modelled cathode catalyst layer and the corresponding cell potential is calculated using Equation (18).

Using realistic values for the nominal cathode overpotential, the PEFC cathode model is repeatedly solved, using the Parametric Sweep utility, to obtain more points in the polarisation curve.

Fig. 5 summarises the algorithm for coupling the agglomerate and PEFC cathode models and Table 2 shows the parameters and constants used in these models. Further, Appendix A lists the input values used for  $\eta$  and  $C_{O_2,o}$  in the agglomerate-scale model.

**[Insert Fig. 4, Fig. 5 and Table 2]**

### 3. Results and discussion

Fig. 6 shows the polarisation curve of the modelled PEFC cathode with the spherical agglomerates. For validation purposes, it is of interest to compare the output of the present model, in which the effects of the catalyst agglomerates are numerically coupled, with that of the conventional agglomerate model, in which the effects of the catalyst agglomerates are analytically coupled. To do so, the polarisation curve using the conventional agglomerate model should be generated. The formula derived to calculate the current density in the conventional model, assuming spherical agglomerates, is the following [53]:

$$\nabla.i = 4F(1 - \varepsilon_{cl})C_{O_2,o} \frac{r_{agg}^3}{(r_{agg} + \delta_{agg})^3} \left( \frac{1}{E_r k} + \frac{\delta_{agg} r_{agg}}{a_{agg}(r_{agg} + \delta_{agg})D_e} \right)^{-1} \quad (20)$$

$$C_{O_2,o} = \frac{C_{O_2,g} RT}{H} \quad (21)$$

where  $C_{O_2,g}$  is the concentration of the gaseous oxygen surrounding the agglomerate before being dissolved into surface of the ionomer film,  $H$  is the Henry's constant,  $r_{agg}$  is the radius of the spherical agglomerate,  $\delta_{agg}$  is the thickness of the ionomer film surrounding the agglomerate and  $a_{agg}$  is the specific surface area of the agglomerate. For the spherical agglomerate,  $a_{agg}$  is given by dividing the surface area of the sphere by the volume of that sphere:

$$a_{agg} = \frac{4\pi r_{agg}^2}{\frac{4}{3}\pi r_{agg}^3} = \frac{3}{r_{agg}} \quad (22)$$

The derived expression for the effectiveness factor  $E_r$  of the spherical agglomerate is given as follows [28, 40]:

$$E_r = \frac{1}{\Phi_L} \left( \frac{1}{\tanh(3\Phi_L)} - \frac{1}{3\Phi_L} \right) \quad (23)$$

$$\Phi_L = \frac{r_{agg}}{3} \sqrt{\frac{k}{D_e^{eff}}} \quad (24)$$

where  $\Phi_L$  is known as the Thiele modulus. Therefore, rather than using Equation (19), Equations (20-24) were used to couple the agglomerate effects into the PEFC cathode model and generate the corresponding current density. Fig. 7 shows that the agreement between the polarisations curves generated by the two approaches is excellent. This imparts confidence in the developed modelling framework.

**[Insert Fig. 6 and Fig. 7]**

We now investigate the sensitivity of the modelled PEFC cathode to the shape of the agglomerate. In the same manner as for the spherical agglomerate,  $\overline{I_{agg}}$  was computed for the cylindrical and cubic agglomerate models and incorporated into the PEFC cathode model. Fig. 8 shows that a slight performance gain is obtained when using the cylindrical agglomerates; the maximum reported current density has increased by only about 5% when changing from spherical agglomerate to cylindrical agglomerate. This is due to the relatively larger specific surface area featured by these agglomerates. The specific surface areas were computed using the software to be about  $6.8 \times 10^7$ ,  $3.7 \times 10^7$  and  $3.0 \times 10^7$   $m^{-1}$  for the cylindrical, cubic and spherical agglomerates, respectively. As stated earlier, the performance gain due to the use of cylindrical agglomerates is slight and this is due to the relatively small size of the agglomerates investigated which mitigates the diffusion resistance.

**[Insert Fig. 8]**

The effects of the agglomerate shape is expected to be larger with larger agglomerate size and this is due to the increased diffusion paths within the agglomerate. To explore this, the investigated agglomerates were scaled up by a factor of 10 and the corresponding polarisation curves were generated; see Fig. 9. It is clear from the figure that the effect of the agglomerate shape is significant this time. A significant performance gain is obtained when using the cylindrical agglomerates; the maximum reported current density has increased by about 60% when changing from the spherical agglomerate to cylindrical agglomerate. With the larger agglomerates, the performance of the modelled PEFC cathode is highly diffusion limited. Under such conditions, the specific surface area, which is significantly larger in the case of cylindrical agglomerates, plays a vital role in improving the fuel cell performance. These results are in accordance with those obtained by Kamarajugadda and Mazumder [8] in which, as mentioned in the introduction, the performance was found to be better with the

overlapping two agglomerates than with a single agglomerate of the same volume as the specific surface area of the former case, i.e. the overlapping two agglomerates, was larger. It should be noted that the scaled-up cylindrical agglomerates were assumed in this study to be parallel to the surface of the catalyst layer facing the GDL and therefore the diffusion path is the diameter of the cylinder. If the cylindrical agglomerates are normal to the surface of the catalyst layer facing the GDL, then the diffusion path will be the height of the scaled-up cylindrical agglomerate (which is of the same order of the thickness of the catalyst layer) and therefore the assumption that this agglomerate is electrically iso-potential is likely to be invalid.

By comparing the polarisation curves in Fig. 8 and Fig. 9, it is clear that the performance of the modelled PEFC cathode is larger with smaller agglomerates. Compared to the large agglomerates, the small agglomerates provide larger specific surface area and subsequently less diffusion resistance.

**[Insert Fig. 9]**

Making use of the flexibility of the present modelling technique, it is of interest to investigate how the changes in the structure of the investigated agglomerates affect the performance. For this purpose, the model of the ‘large’ cubic agglomerate was selected. Namely, it was made perforated by creating three circular holes, with about 120 nm radius, in all the principal directions; see Fig. 10. Upon solving the modelled PEFC cathode model with the above modified cubic agglomerate, the corresponding polarisation curve was generated. Fig. 11 shows that such a slight modification to the cubic agglomerate has significantly improved the performance of the modelled PEFC cathode. This improvement is attributed to the significant increase in the specific surface area of the agglomerate; it has increased from about  $3.7 \times 10^6$

$\text{m}^{-1}$  in the original cubic agglomerate to about  $10.5 \times 10^6 \text{ m}^{-1}$  in the modified cubic agglomerate.

Finally, it should be noted that one may be able to predict which agglomerate will perform the best based on the specific area. However, quantifying the performance gain is one the appealing features of the multiscale modelling framework especially when modelling agglomerates with much more complicated structures same as those described in [61].

**[Insert Fig. 10 and Fig. 11]**

## **4. Conclusions**

In this paper, a multiscale modelling framework is developed for the PEFC cathode electrode. This framework aims at unlocking the limitations associated with the use of the classical agglomerate model where the effects of the microstructure of the agglomerate are analytically incorporated into the fuel cell-scale model. With the developed modelling framework, such microstructure effects are numerically coupled through consecutively solving an agglomerate-scale model and a cell-scale model. Namely, the agglomerate-scale model is firstly solved to generate the data that are required to be fed into the cell-scale model to generate the performance curves. To this end, one can freely investigate the structure of the agglomerate without being limited to the three shapes dictated by using the conventional agglomerate model: spheres, long cylinders with sealed ends and long slabs with sealed ends.

To demonstrate the practicality of the developed modelling framework, three agglomerates of different shapes but with the same volume have been investigated: spherical, cubic and cylindrical. The developed multi-scale model has been first validated through comparing its output with that of the classical agglomerate model. The agreement between the corresponding polarisation curves was found to be excellent. The performance of the modelled PEFC cathode was shown to be slightly sensitive to the shape of the agglomerate

when the size of the latter is relatively small (i.e. of the order of 100 nm) and this is due to the relatively low diffusion resistance. The maximum reported current density has only increased by about 5% when changing from the spherical agglomerate to the cylindrical agglomerate. However, the effects of the agglomerate shape become much more profound with larger agglomerates (i.e. of the order of 1000 nm) as the cathode electrode becomes more diffusion limited especially at high current densities. In such a situation, the best performance is obtained by the agglomerate with the highest specific surface area which is, amongst the investigated agglomerates, the cylindrical agglomerate; the maximum reported current density has increased by about 60% when changing from the spherical agglomerate to the cylindrical agglomerate. Further, it was shown that a slight change to the structure of the agglomerate may have a significant effect on the fuel cell performance; the performance of the PEFC cathode has been significantly improved when perforating the relatively large cubic agglomerate with few holes.

## Nomenclature

a	Specific surface area of platinum catalyst	$\text{m}^{-1}$
$a_{\text{agg}}$	Specific surface area of agglomerate	$\text{m}^{-1}$
$A_{\text{pt}}$	Electrochemical surface area of platinum catalyst	$\text{m}^2/\text{kg}$
C	Molar concentration	$\text{mol m}^{-3}$
D	Diffusivity	$\text{m}^2 \text{s}^{-1}$
$E_{\text{cell}}$	Cell potential	V
$E_{\text{th}}$	Theoretical cell potential	V
F	Faraday's constant	$\text{C mol}^{-1}$
H	Henry's constant	$\text{atm m}^3 \text{mol}^{-1}$
i	Current density	$\text{A m}^{-2}$
$i_0$	Exchange current density	$\text{A m}^{-2}$
k	Reaction rate constant	$\text{s}^{-1}$

L	Thickness	m
$l_{pt}$	Platinum loading	$\text{kg m}^{-2}$
M	Molecular weight	$\text{kg m}^{-3}$
nd	Net drag coefficient	-
N	Mass flux	$\text{kg m}^{-2} \text{ s}^{-1}$
p	Pressure	Pa
$r_{agg}$	Radius of spherical agglomerate	m
R	Universal gas constant	$\text{J K}^{-1} \text{ mol}^{-1}$
$R_{\text{rxn}, \text{O}_2}$	Reaction rate of oxygen consumption	$\text{mol m}^{-3} \text{ s}^{-1}$
T	Temperature	K
w	Mass fraction	-
x	Mole fraction	-
V	Volume of agglomerate	$\text{m}^3$

### Greek symbols

$\alpha$	Charge transfer coefficient	-
$\varepsilon$	Porosity/volume fraction	-
$\eta$	Overpotential	V
$\Phi_L$	Thiele modulus	-
$\sigma$	Conductivity	$\text{S m}^{-1}$
$\delta_{agg}$	Thickness of ionomer film	m
$\phi$	Potential	V
$\rho$	Density	$\text{kg m}^{-3}$

### Subscripts and superscripts

agg	Agglomerate
cl	Catalyst layer
eff	Effective
g	Gas
j	Component j

k	Component k
m	Membrane
pt	Platinum
ref	Reference
S	Solid phase/solid surface

## Appendix A

Below are the values used for the input variables of  $\eta$  and  $C_{O_2,o}$  in the agglomerate-scale model. Note that the total number of simulations is the multiplication product of the number of values for  $\eta$  and the number of values for  $C_{O_2,o}$ , namely  $19 \times 20$ . For the given meshed computational domains of the investigated agglomerates, the completion of the entire set of simulations takes about 1-2 hours.

**[Insert Table A.1]**

## References

- [1] Litster S, Epting WK, Wargo EA, Kaliadindi SR, Kumber EC. Morphological Analyses of Polymer Electrolyte Fuel Cell Electrodes with Nano-Scale Computed Tomography Imaging. *Fuel Cells* 2013;13:935-45.
- [2] Carton JG, Olabi AG. Three-dimensional proton exchange membrane fuel cell model: Comparison of double channel and open pore cellular foam flow plates. *Energy*, In Press: <http://dx.doi.org/10.1016/j.energy.2016.02.010>.
- [3] Fofana D, Natarajan SK, Hamelin J, Benard P. Low platinum, high limiting current density of the PEMFC (proton exchange membrane fuel cell) based on multilayer cathode catalyst approach. *Energy* 2014;64:398-403.
- [4] Avasarala B, Haldar P. Durability and degradation mechanism of titanium nitride based electrocatalysts for PEM (proton exchange membrane) fuel cell applications. *Energy* 2013;57:545-53.
- [5] Middelmann E. Improved PEM fuel cell electrodes by controlled self-assembly. *Fuel Cells Bulletin* 2002;11:9-12.
- [6] Antolini E. Carbon supports for low-temperature fuel cell catalysts. *Appl Catalysis B: Environmental* 2009;88:1-24.
- [7] Esmaeilifar A. Synthesis methods of low-Pt-loading electrocatalysts for proton exchange membrane fuel cell systems. *Energy* 2010;35:3941-57.
- [8] Kamarajugadda S, Mazumder S. Generalized flooded agglomerate model for the cathode catalyst layer of a polymer electrolyte membrane fuel cell. *J Power Sources* 2012;208:328-39.
- [9] Ismail MS, Ingham DB, Hughes KJ, Ma L, Pourkashanian M. The effects of shape on the performance of cathode catalyst agglomerates in polymer electrolyte fuel cells: a micro-scale FEM study. *Int J Numerical Methods Heat Fluid Flow* 2016;26:1145-56.
- [10] Siegel C. Review of computational heat and mass transfer modeling in polymer-electrolyte-membrane (PEM) fuel cells. *Energy* 2008;33:1331-52.

- [11] Djilali N. Computational modelling of polymer electrolyte membrane (PEM) fuel cells: Challenges and opportunities. *Energy* 2007;32:269-80.
- [12] Berning T, Djilali N. A 3D, Multiphase, Multicomponent Model of the Cathode and Anode of a PEM Fuel Cell. *J Electrochem Soc* 2003;150:A1589-98.
- [13] Berning T, Lu DM, Djilali N. Three-dimensional computational analysis of transport phenomena in a PEM fuel cell. *J Power Sources* 2002;106:284-94.
- [14] Ismail MS, Ingham DB, Hughes KJ, Ma L, Pourkashanian M. An efficient mathematical model for air-breathing PEM fuel cells. *Appl Energy* 2014;135:490-503.
- [15] Belkhir Z, Zeroual M, Moussa HB, Zereg M, Zitouni B. Numerical simulation of exchange membrane fuel cells in different operating conditions. *Int J Hydrogen Energy* 2012;37:5444-51.
- [16] Cordiner S, Lanzani SP, Mulone V. 3D effects of water-saturation distribution on polymeric electrolyte fuel cell (PEFC) performance. *Int J Hydrogen Energy* 2011;36:10366-75.
- [17] Xing L, Mamlouk M, Kumar R, Scott K. Numerical investigation of the optimal Nafion® ionomer content in cathode catalyst layer: An agglomerate two-phase flow modelling. *Int J Hydrogen Energy* 2014;39:9087-104
- [18] Carcadea E, Ene H, Ingham DB, Lazer R, Pourkashanian M, Stefanescu I. *Int J Numerical Methods Heat Fluid Flow* 2007;17:302-12.
- [19] Ismail MS, Hughes KJ, Ingham DB, Ma L, Pourkashanian M. Effects of anisotropic permeability and electrical conductivity of gas diffusion layers on the performance of proton exchange membrane fuel cells. *Appl Energy* 2012;95:50-63.
- [20] Kulikovskiy AA, Divisek J, Kornyshev AA. Modeling the Cathode Compartment of Polymer Electrolyte Fuel Cells: Dead and Active Reaction Zones. *J Electrochem Soc* 1999;146:3981-91.
- [21] Meng H, Wang CY. Electron Transport in PEFCs. *J Electrochem Soc* 2004;151:A358-A67.

- [22] Song D, Wang Q, Liu Z, Navessin T, Eikerling M, Holdcroft S. Numerical optimization study of the catalyst layer of PEM fuel cell cathode. *J Power Sources* 2004;126:104-11.
- [23] Um S, Wang CY. Three-dimensional analysis of transport and electrochemical reactions in polymer electrolyte fuel cells. *J Power Sources* 2004;125:40-51.
- [24] Zhou T, Liu H. A 3D model for PEM fuel cells operated on reformat. *J Power Sources* 2004;138:101-10.
- [25] Ramos-Alvarado B, Hernandez-Guerrero A, Juarez-Robles D, Li P. Numerical investigation of the performance of symmetric flow distributors as flow channels for PEM fuel cells. *Int J Hydrogen Energy* 2012;37:436-48
- [26] Alhazmi, N., Ingham DB, Ismail MS, Hughes KJ, Ma L, Pourkashanian M. Effect of the anisotropic thermal conductivity of GDL on the performance of PEM fuel cells. *Int J Hydrogen Energy* 2013;37:603-11.
- [27] Rakhshanpouri S, Rowshanzamir S. Water transport through a PEM (proton exchange membrane) fuel cell in a seven-layer model. *Energy* 2013;50:220-31.
- [28] Ismail MS, Ingham DB, Hughes KJ, Ma L, Pourkashanian M. Effective diffusivity of polymer electrolyte fuel cell gas diffusion layers: An overview and numerical study. *Int J Hydrogen Energy* 2015;40:10994-1010.
- [29] Moein-Jahromi M, and Kermani MJ. Performance prediction of PEM fuel cell cathode catalyst layer using agglomerate model. *Int J Hydrogen Energy* 2012;37:17954-66.
- [30] Secanell M, Karan K, Suleman A, Djilali N. Multi-variable optimization of PEMFC cathodes using an agglomerate model. *Electrochim Acta* 2007;52:6318-37.
- [31] Siegel NP, Ellis MW, Nelson DJ, von Spakovsky MR. Single domain PEMFC model based on agglomerate catalyst geometry. *J Power Sources* 2003;115:81-9.
- [32] Broka K, Ekdunge P. Modelling the PEM fuel cell cathode. *J Appl Electrochem* 1997; 27:281-9.

- [33] Cetinbas FC, Advani SG, Prasad AK. A Modified Agglomerate Model with Discrete Catalyst Particles for the PEM Fuel Cell Catalyst Layer. *J Electrochem Soc* 2013;160:F750-6.
- [34] Cetinbas FC, Advani SG, Prasad AK. Three dimensional proton exchange membrane fuel cell cathode model using a modified agglomerate approach based on discrete catalyst particles. *J Power Sources* 2014;250:110-19.
- [35] Jain P, Biegler LT, Jhon MS. Sensitivity of PEFC Models to Cathode Layer Microstructure. *J Electrochem Soc* 2010;157:B1222-B9.
- [36] Jaouen F, Lindbergh G, Sundholm G. Investigation of Mass-Transport Limitations in the Solid Polymer Fuel Cell Cathode: I. Mathematical Model. *J Electrochem Soc* 2002;149:A437-A47.
- [37] Kamarajugadda S, Mazumder S. Numerical investigation of the effect of cathode catalyst layer structure and composition on polymer electrolyte membrane fuel cell performance. *J Power Sources* 2008;183:629-42.
- [38] Rao RM, Rengaswamy R. Dynamic characteristics of spherical agglomerate for study of cathode catalyst layers in proton exchange membrane fuel cells (PEMFC). *J Power Sources* 2006;158:110-23.
- [39] Obut S, Alper E. Numerical assessment of dependence of polymer electrolyte membrane fuel cell performance on cathode catalyst layer parameters. *J Power Sources* 2011;196:1920-31.
- [40] Sun W, Peppley BA, Karan K. An improved two-dimensional agglomerate cathode model to study the influence of catalyst layer structural parameters. *Electrochim Acta* 2005;50:3359-74.
- [41] Wang Q, Eikerling M, Song D, Liu Z. Structure and performance of different types of agglomerates in cathode catalyst layers of PEM fuel cells. *J Electroanalytic Chem* 2004.;573:61-9.
- [42] Yin KM. Parametric Study of Proton-Exchange-Membrane Fuel Cell Cathode Using an Agglomerate Model. *J Electrochem Soc* 2005;152:A583-A93.

- [43] Tabe Y, Nishino M, Takamatsu H, Chikahisa T. Effects of Cathode Catalyst Layer Structure and Properties Dominating Polymer Electrolyte Fuel Cell Performance. *J Electrochem Soc* 2011;158:B1246-B54.
- [44] Yoon W, and Weber AZ. Modeling Low-Platinum-Loading Effects in Fuel-Cell Catalyst Layers. *J Electrochem Soc* 2011;158:B1007-B18.
- [45] Cetinbas FC, Advani SG, Prasad AK. An Improved Agglomerate Model for the PEM Catalyst Layer with Accurate Effective Surface Area Calculation Based on the Sphere-Packing Approach. *J Electrochem Soc* 2014;161:F803-F13.
- [46] Xing L, Qiong C, Xu C, Liu C, Scott K, Yan Y. Numerical study of the effect of relative humidity and stoichiometric flow ratio on PEM (proton exchange membrane) fuel cell performance with various channel lengths: An anode partial flooding modelling. *Energy* 2016;106:631-45.
- [47] Xing, L, Du S, Chen R, Mamlouk M, Scott K. Anode partial flooding modelling of proton exchange membrane fuel cells: Model development and validation. *Energy* 2016; 96:80-95.
- [48] Xing L, Liu X, Alaje T, Kumar R, Mamlouk M, Scott K. A two-phase flow and non-isothermal agglomerate model for a proton exchange membrane (PEM) fuel cell. *Energy* 2014;73:618-34.
- [49] Xing L, Mamlouk M, Scott K. A two dimensional agglomerate model for a proton exchange membrane fuel cell. *Energy* 2013;61:196-210.
- [50] Aris R. On shape factors for irregular particles—I: The steady state problem. *Diffusion and reaction. Chem Eng Sci*;1957:262-8.
- [51] Thiele EW. Relation between Catalytic Activity and Size of Particle. *Ind Eng Chem* 1939;31:916-20.
- [52] Marthosa S. Improvement of electrocatalyst performance in hydrogen fuel cells by multi-scale modelling. PhD Thesis, University of Manchester (2012), Manchester.

- [53] Moore M, Wardlaw P, Dobson P, Boisvert JJ, Putz A, Spiteri RJ, Secanell M. Understanding the Effect of Kinetic and Mass Transport Processes in Cathode Agglomerates. *J Electrochem Soc* 2014;161:E3125-E37.
- [54] Du S, Pollet BG. "Application of Nanometariesl in Fuel Cells" in *Nanotechnology for Sustainable Manufacturing*, Editor: Rickerby D. CRC Press (2014).
- [55] Chang H, Joo SH, Pak C. Synthesis and characterization of mesoporous carbon for fuel cell applications. *J Materials Chem* 2007;17:3078-88.
- [56] Knupp SL, Li W, Paschos O, Murray TM, Synder J, Halder P. The effect of experimental parameters on the synthesis of carbon nanotube/nanofiber supported platinum by polyol processing techniques. *Carbon* 2008;46:1276-84.
- [57] Sun Y, Wu Q, Shi G. Graphene based new energy materials. *Energy & Environ Sci* 2011;4:1113-32.
- [58] Antolini E, Gonzalez ER. Polymer supports for low-temperature fuel cell catalysts. *Applied Catalysis A: General* 2009;365:1-19.
- [59] Pylypenko S, Olson TS, Carroll NJ, Petsev DN, Atanassov P. Templated Platinum/Carbon Oxygen Reduction Fuel Cell Electrocatalysts. *J Phys Chem C* 2010;114:4200-7.
- [60] Balgis R, Anilkumar GM, Sago S, Ogi T, Okuyama K. Nanostructured design of electrocatalyst support materials for high-performance PEM fuel cell application. *J Power Sources* 2012;203:26-33.
- [61] Kongkanand A, Mathias MF. The Priority and Challenge of High-Power Performance of Low-Platinum Proton-Exchange Membrane Fuel Cells. *J Phys Chem Letters* 2016;7:1127-37.

## Figure Captions

**Fig. 1** A cut through the modelled spherical agglomerate that shows the boundary conditions.

**Fig. 2** The meshed computational domains of the investigated agglomerates: a sphere (left), long cylinder (middle) and cube (right). Note that only one eighth of each agglomerate has been modelled, making use of the symmetry existing in the investigated agglomerates.

**Fig. 3** A schematic diagram of the PEFC cathode model with the prescribed boundary conditions. Note that the subscript  $j$  represent the chemical species involved: oxygen nitrogen and water vapour.

**Fig. 4** The averaged current density of the agglomerate  $\overline{I_{agg}}$  as a function of overpotential and concentration at the surface of the ionomer film covering the spherical agglomerate with a radius of (a) 100 nm and (b) 1000 nm.

**Fig. 5** The algorithm used to couple and solve the agglomerate and PEFC cathode models.

**Fig. 6** The polarisation curve of the modelled PEFC cathode with the spherical agglomerates.

**Fig. 7** The polarisation curves generated from the modelled PEFC cathode with the numerical coupling of the agglomerate effects (solid line) and the analytical coupling of these effects (dashed line) for an agglomerate radius of (a) 100 nm and (b) 1000 nm.

**Fig. 8** The polarisation curves generated from the modelled PEFC cathode with cylindrical agglomerates (solid line), cubic agglomerates (dashed line) and spherical agglomerate (dotted line).

**Fig. 9** The polarisation curves generated from the modelled PEFC cathode with the scaled-up: cylindrical agglomerates (solid line), cubic agglomerates (dashed line) and spherical agglomerate (dotted line).

**Fig. 10** The perforated 'large' cubic agglomerate.

**Fig. 11** The polarisation curves generated from the modelled PEFC cathode with the modified cubic agglomerates (solid line) and original cubic agglomerates (dotted line).

## Tables

**Table 1 The dimensions of the investigated agglomerates.**

<b>Agglomerate</b>	<b>Dimensions</b>
Sphere	Radius = 100 nm
Cube	Side length/2 ~ 80.5 nm
Long cylinder	Radius ~ 32 nm Height ~ 40 × Radius

**Table 2 List of the constants and physical parameters used in the models.**

Parameter	Value
Faradays' constant, $F$	96485 C mol <sup>-1</sup>
Universal gas constant, $R$	8.314 J mol <sup>-1</sup> K <sup>-1</sup>
Electrochemical surface area of platinum catalyst, $A_{pt}$	40 m <sup>2</sup> g <sup>-1</sup> [44]
Temperature, $T$	353 K
Pressure, $p$	1.5 atm
Total concentration	51.77 mol m <sup>-3</sup>
Oxygen/nitrogen molar ratio	0.21/0.79
Inlet concentration of water vapour	8.10 mol m <sup>-3</sup>
Thickness of GDL	250 μm
Thickness of catalyst layer, $L_{cl}$	15 μm
GDL porosity, $\varepsilon$	0.6
Porosity of catalyst layer, $\varepsilon_{cl}$	0.48 <sup>a</sup>
Platinum loading, $l_{pt}$	0.4 mg cm <sup>-2</sup>
Oxygen diffusivity in the ionomer, $D_e$	$8.45 \times 10^{-10}$ m <sup>2</sup> s <sup>-1</sup> [40]
Henry's constant for oxygen in the ionomer, $H$	0.3125 atm m <sup>3</sup> mol <sup>-1</sup> [40]
Effective electrical conductivity of GDL, $\sigma_{GDL}^{eff}$	100 S m <sup>-1</sup> [40]
Effective electrical conductivity of catalyst layer, $\sigma_{cl}^{eff}$	30 S m <sup>-1</sup> [40]
Effective ionic conductivity of electrolyte, $\sigma_m^{eff}$	0.8 S m <sup>-1</sup> <sup>b</sup>
Ionomer volume fraction in the agglomerate, $\varepsilon_e$	0.5
Reference concentration of dissolved oxygen, $C_{O_2}^{ref}$	0.85 mol m <sup>-3</sup> [40]
Binary diffusivity of oxygen in nitrogen, $D_{O_2-N_2}$	$1.86 \times 10^{-5}$ m <sup>2</sup> s <sup>-1</sup> [40]
Binary diffusivity of water vapour in nitrogen, $D_{H_2O-N_2}$	$2.58 \times 10^{-5}$ m <sup>2</sup> s <sup>-1</sup> [40]
Binary diffusivity oxygen in water vapour, $D_{O_2-H_2O}$	$2.47 \times 10^{-5}$ m <sup>2</sup> s <sup>-1</sup> [40]
Exchange current density, $i_o$	0.015 A m <sup>-2</sup> [40]
Charge transfer coefficient, $\alpha$	0.61 [40]

<b>Net drag coefficient, nd</b>	$1 \ (\eta < 0.25V)$
	$46\eta^2 - 31.52\eta + 5.7$ $(0.25V \leq \eta \leq 0.35V)$
	$0.3 \ (\eta > 0.35V) \ [40]$

<sup>a</sup> This is the porosity obtained for the cubic packing arrangement for the spherical agglomerates [45]. For comparative purposes, the same porosity value was used when using the cubic and the cylindrical agglomerates.

<sup>b</sup> Calculated using the Springer model and considering the fraction of the ionomer in the agglomerate.

**Table A.1 The values of  $\eta$  and  $C_{O_2,o}$  used in the agglomerate-scale model.**

<b>Number</b>	$\eta$	<b>Number</b>	$C_{O_2,o}$
1	-0.10	1	1.00E-12
2	-0.15	2	0.045263
3	-0.20	3	0.090526
4	-0.25	4	0.13579
5	-0.30	5	0.18105
6	-0.35	6	0.22632
7	-0.4	7	0.27158
8	-0.45	8	0.31684
9	-0.50	9	0.36211
10	-0.55	10	0.40737
11	-0.60	11	0.45263
12	-0.65	12	0.49789
13	-0.70	13	0.54316
14	-0.75	14	0.58842
15	-0.80	15	0.63368
16	-0.85	16	0.67895
17	-0.90	17	0.72421
18	-0.95	18	0.76947
19	-1.0	19	0.81474
		20	0.86000

**Figure 1**

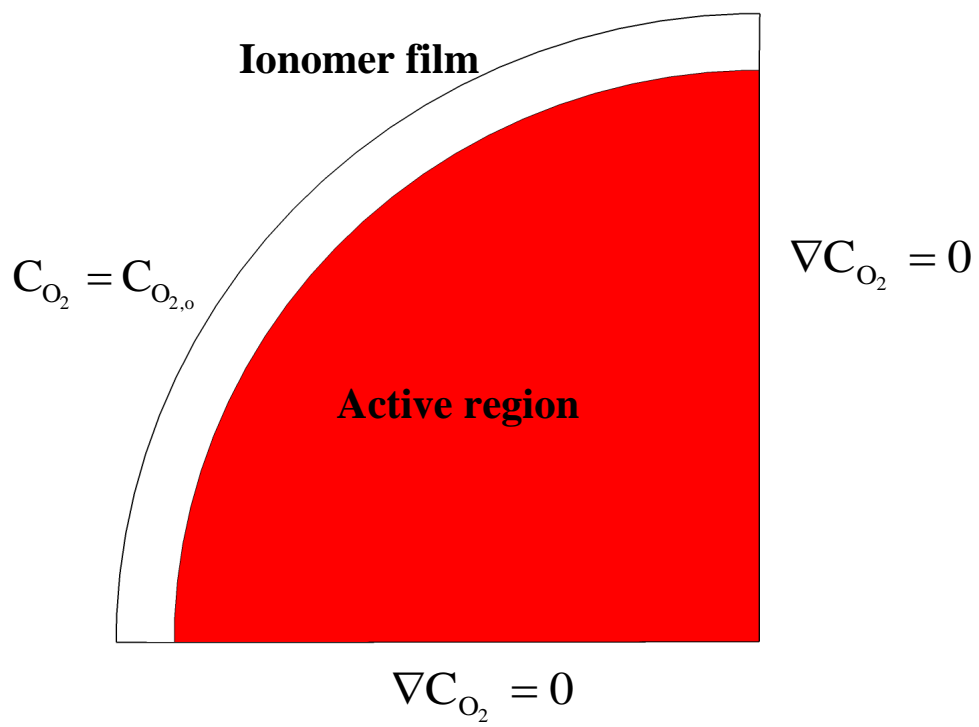


**Figure 2**

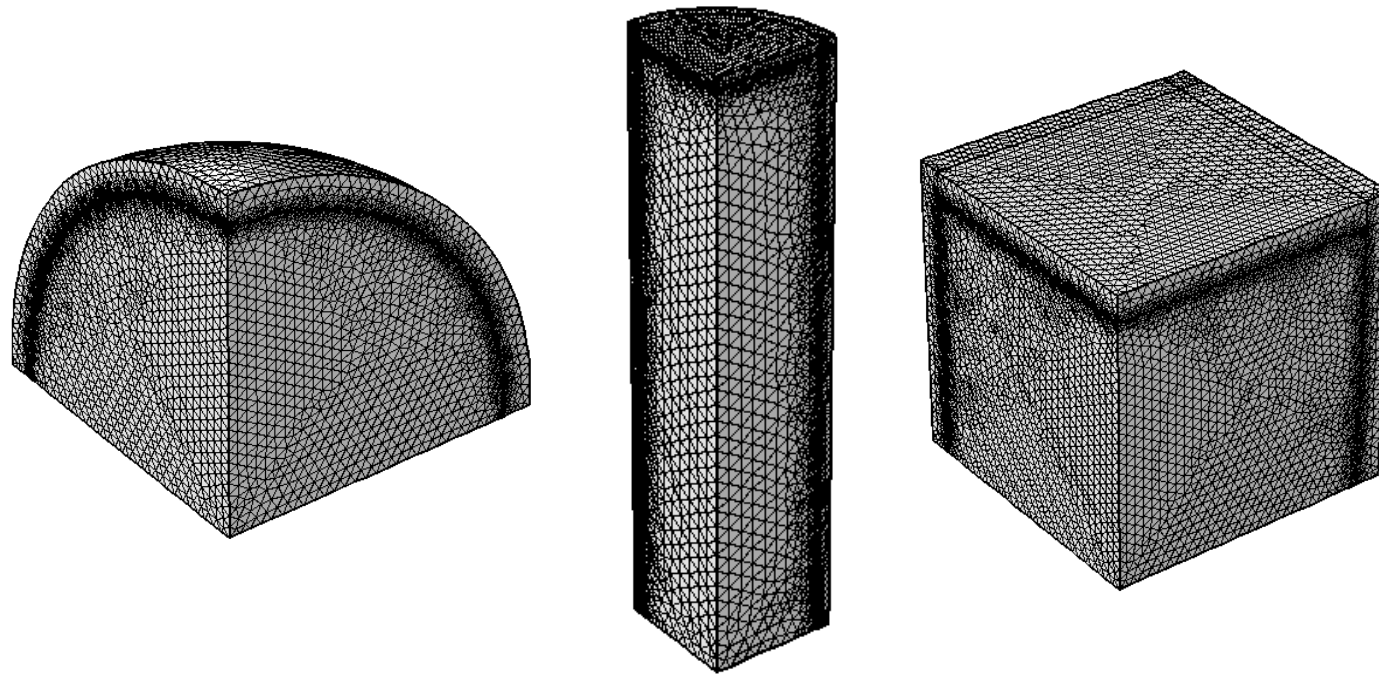


**Figure 3**

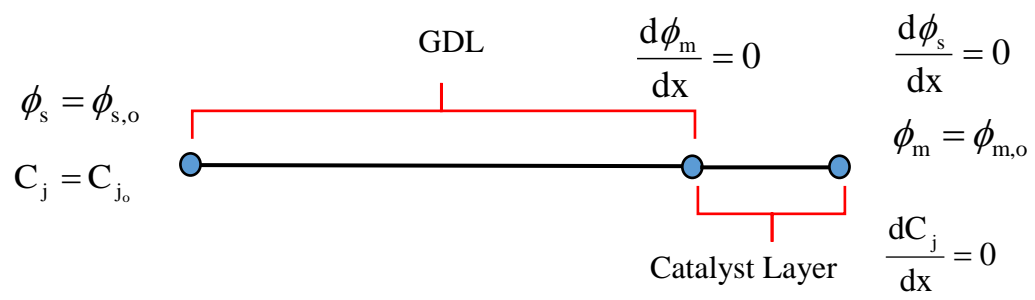
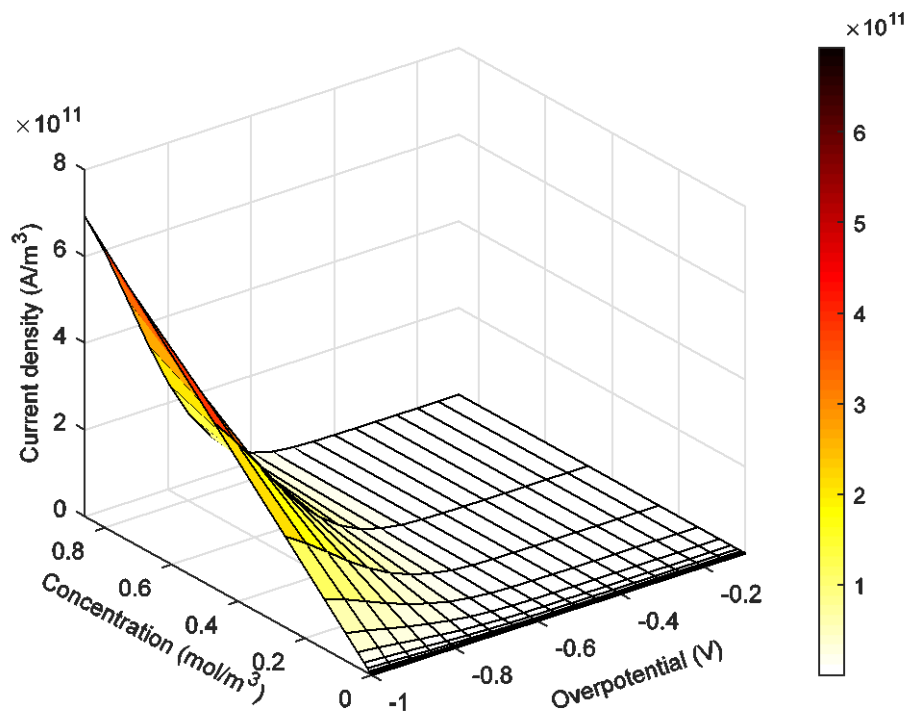
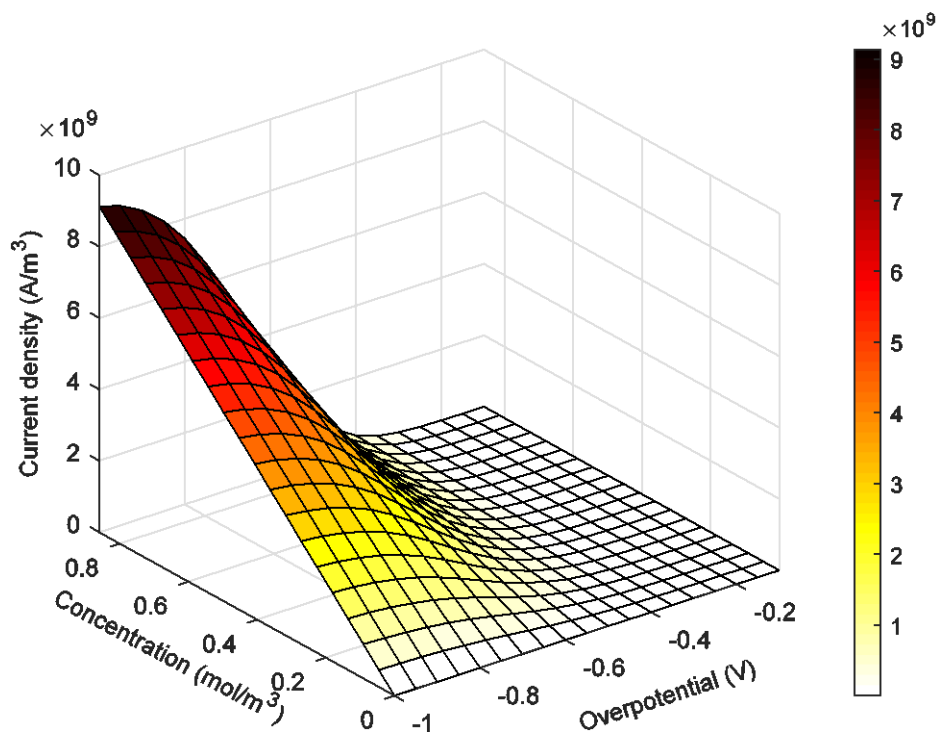


Figure 4



(a)



(b)

**Figure 5**

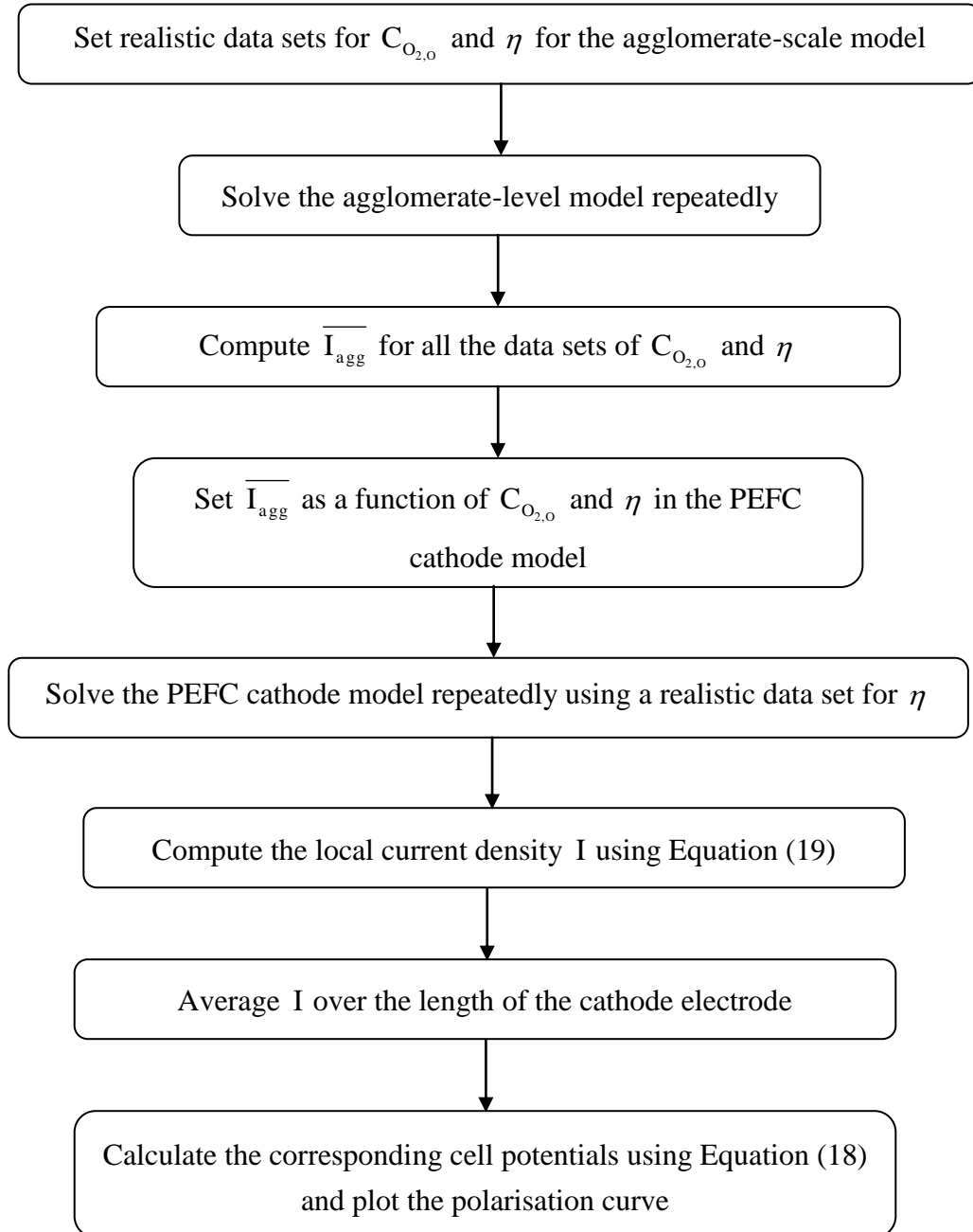


**Figure 6**

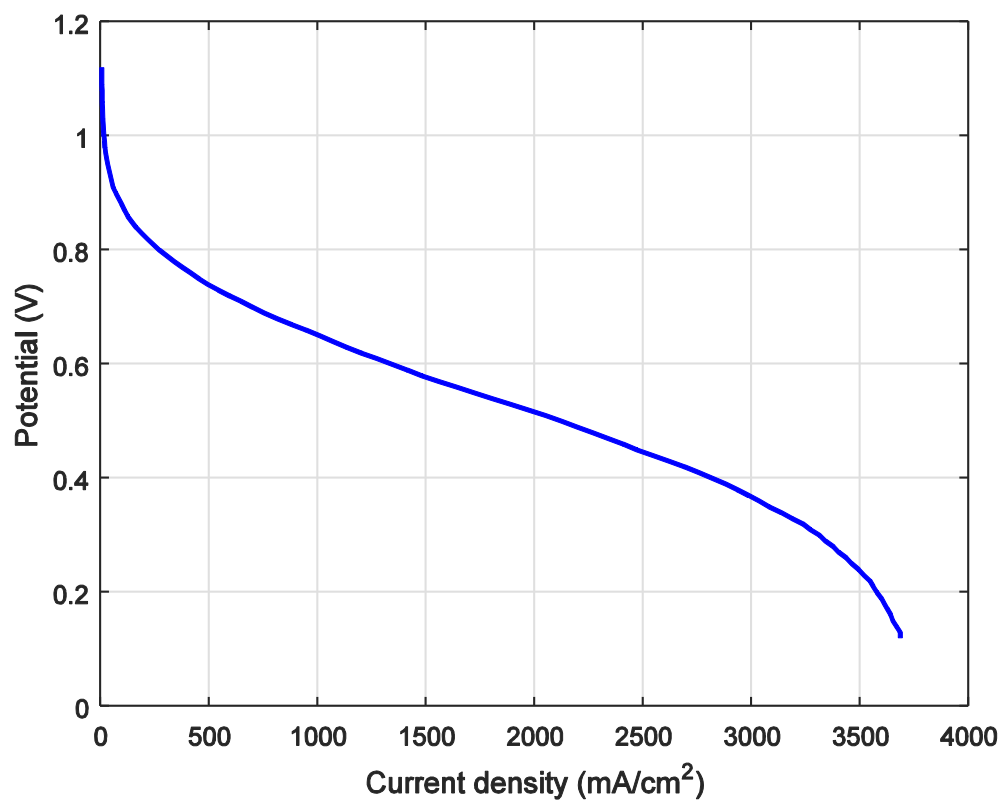
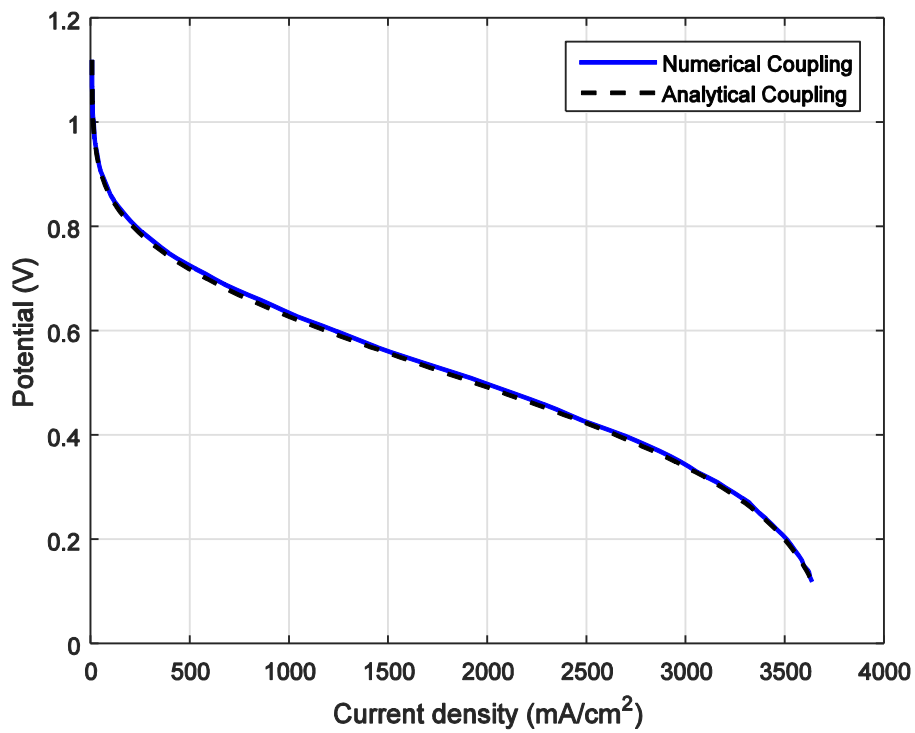
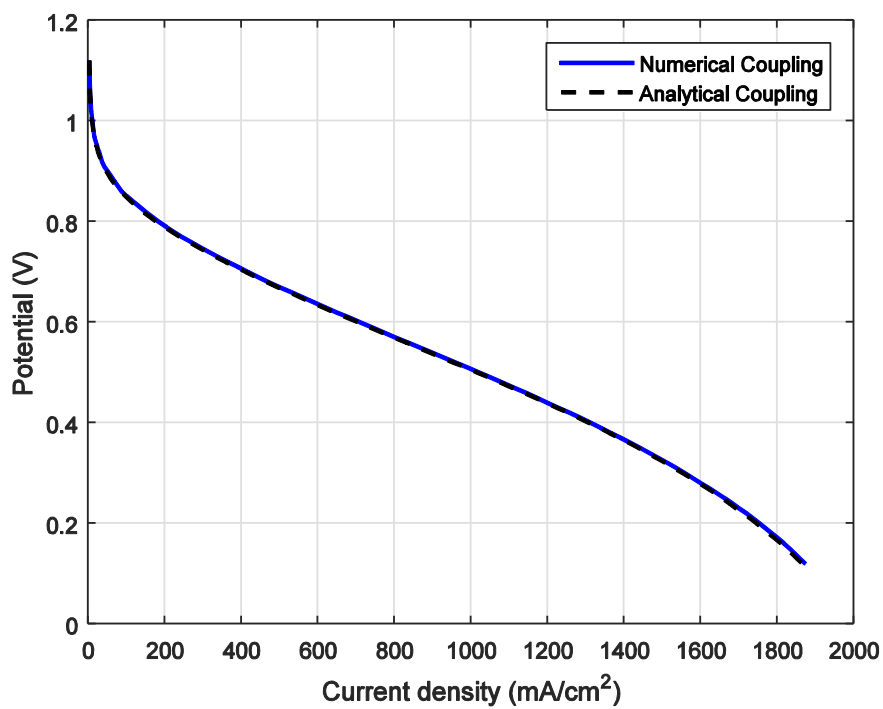


Figure 7



(a)



(b)

Figure 8

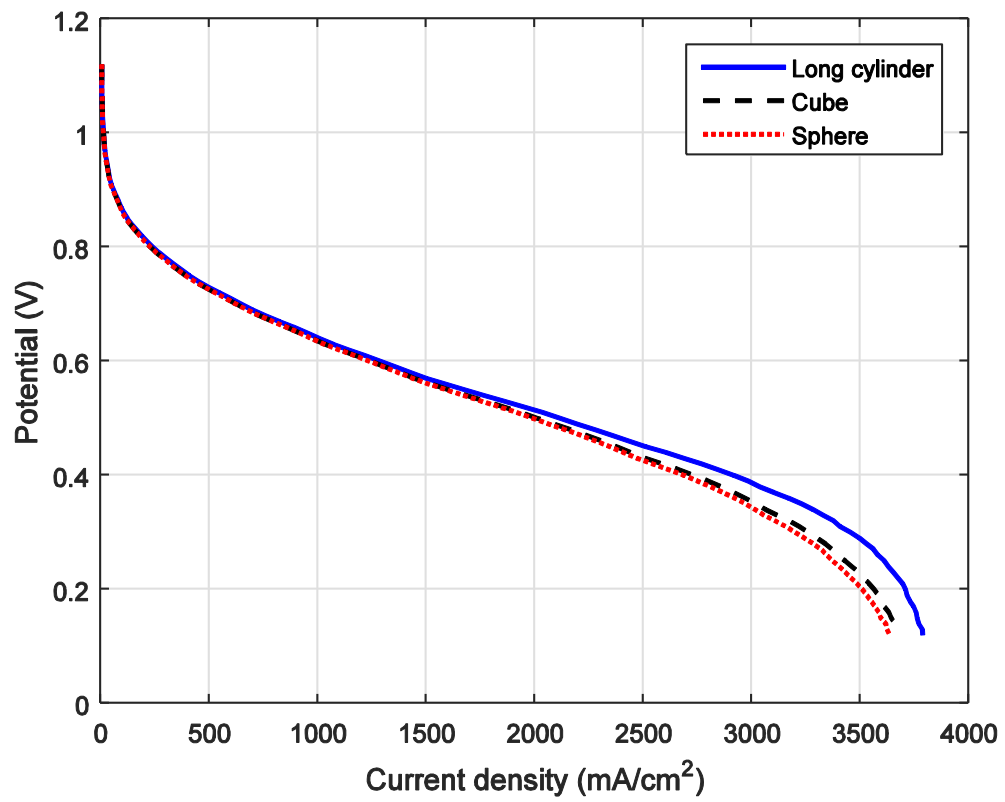
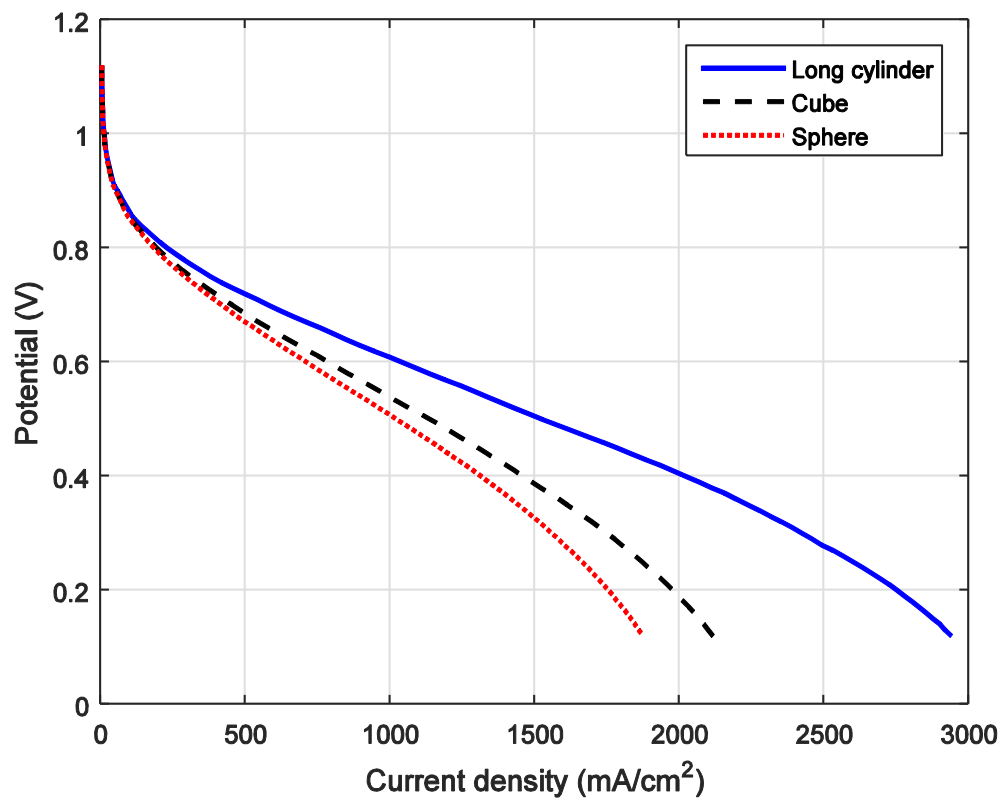
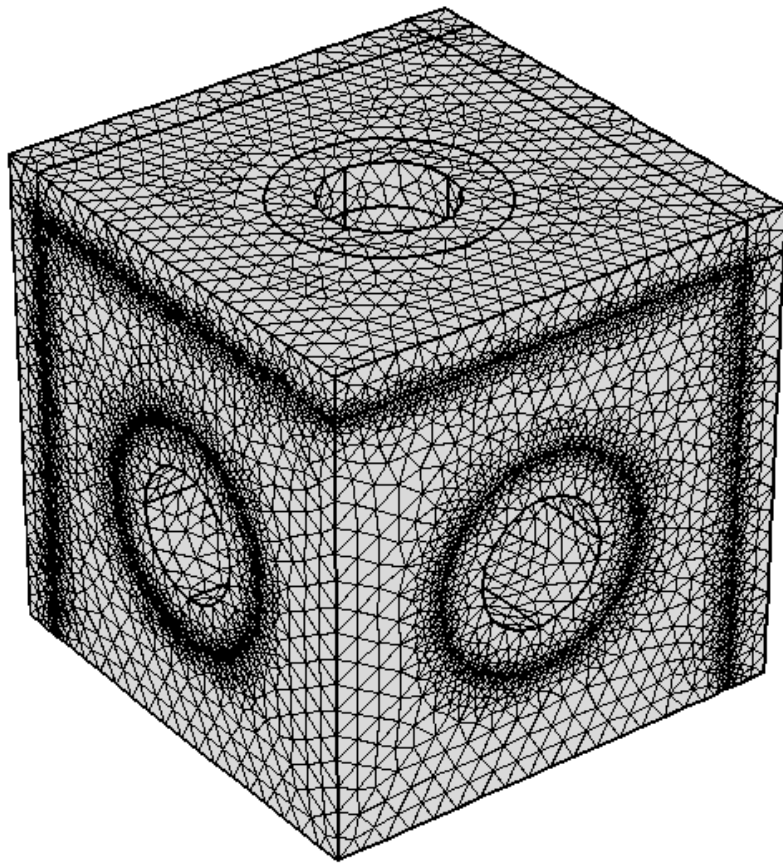


Figure 9



**Figure 10**



**Figure 11**

